SIMULATION OF SOIL NAIL'S DYNAMIC PULLOUT RESPONSE

Assoc. Prof. Tan Siew Ann, National University of Singapore & Mr. Ooi Poh Hai, National University of Singapore & Mr. Cheang Wai Lum, National University of Singapore

INTRODUCTION

The assessment of an in-situ nail – soil interface resistance and its load displacement characteristic are the main design parameters to ensure the stability and serviceability of a nail reinforced structure. Sufficient field pullout results are required for a safe and economic nailed structure design. However, the number of available pullout test results are always limited by time. In view of this, an attempt was initiated at the National University of Singapore to explore the viability of using dynamic pullout tests as an alternative test method to assess the nail's static pullout behavior, because dynamic pullout tests appear to be faster than the conventional quasi static pullout tests.

Before the prototype physical experiment for a dynamic nail pullout test will be carried out, a numerical analysis by 'Plaxis 8.2' was carried out to numerically understand the nail's dynamic pullout behavior and to reveal the effect of a different loading duration. Although it is termed as a dynamic pullout test here, the simulated dynamic loading characteristic is similar to a kinetic (Statnamic) pile load test condition with relative wave length > 10 (Holeyman, 1992).

FINITE ELEMENT MODEL AND MATERIAL PROPERTIES

The horizontally oriented soil nail was modeled as a vertical inclusion in the middle of a soil drum, using the possibilities of the axisymmetry model. The numerical model is shown in Figure 1. For simple comparison between the dynamic and static pullout characteristics, uniform soil conditions were assumed. The horizontal boundary was positioned at a distance of 60r (r = nail's radius) away (Randolph and Wroth, 1978) from the axis of symmetry. The upper vertical boundary was placed at 20r from the nail's head to sufficiently eliminate boundary confinement effects. An absorbent boundary was placed at the right and bottom boundary to eliminate any spurious reflected waves. Table 1 shows the material types and material properties used in the analysis.

Properties	Soil	Nail (steel)
Material model	Mohr Coulomb	Linear elastic
Elastic modulus	10MPa	200GPa
Poisson's ratio	0.3	0.2
Unit weight	18 kN/m^3	80 kN/m^3
Friction angle	36°	-
Cohesion	0°	-
Dilation angle	0°	-
Rinter	0.75	-

Table 1: Material properties

INITIAL STRESS CONDITION

The ground water condition was assumed to be dry. $\sum$-M_{weight} was set to zero in the initial stress generation calculation step in order to avoid initial stresses generated by gravity. The initial stress condition was created by imposing load B (Figure 1) at the right boundary in the first step of calculation; creating a uniformly distributed normal stress along the nail's shaft to simulate the initial stress condition for the actual, horizontally, oriented nail. In this calculation step, the absorbent boundary was deleted, the upper and bottom boundaries were vertically fixed, the left boundary was totally fixed and the right boundary was totally free to allow the imposed load to transfer to the nail's shaft. Interface elements were turned off in this calculation step.

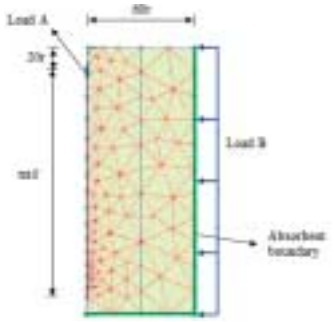

Figure 1.

Due to the characteristics of the axisymmetry model, the generated normal stress with the abovementioned method is uniformly distributed on the nail's perimeter. Although this initial stress condition is different compared to the actual working nail in which the circumferential normal stress distribution is non-uniform, caused by the difference in vertical and horizontal stress, this shortcoming does not cause severe errors because the main purpose of this study is to compare the differences between static and dynamic pullout response of the modeled soil nail under the same conditions.

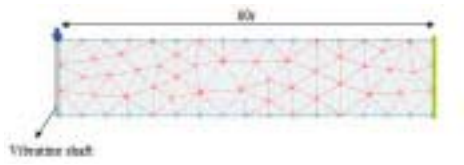

Figure 2.

DYNAMIC STIFFNESS AND DAMPING COEFFICIENT

According to the Plaxis 8 dynamic manual, radiation (geometry) damping, which will happen naturally in a numerical calculation, is the dominant damping effect for a single source problem with an axisymmetric model, and Rayleigh damping can be ignored. This statement agrees with the finding by other researchers such as Chow Y.K. (1981) who concluded that radiation damping is the dominant damping source in pile driving. In order to assess the accuracy of Plaxis 8.2 in the modeling of radiation damping, the dynamic response of a circular soil disk with a massless vibrating shaft at the axis of symmetry, as shown in Figure 2, was calculated. A known frequency harmonic load was imposed on the shaft and the calculated vibration response was measured. According to the dynamic equation of motion as shown below,

$$Ma + Cv + Ku = F$$

with M = 0, the dynamic stiffness (K) and damping (C) coefficient can be back-calculated by matching the measured displacement (u) and velocity (v) with the imposed

harmonic load (F). Figure 3 shows the back-analyzed stiffness and damping coefficient plotted against a dimensionless frequency, a_0, defined as

$$a_0 = \frac{r\varpi}{V_s}$$

With r = the shaft's radius, ϖ = the circular frequency and V_s = the soil's distortion stress velocity.
The theoretical value for the stiffness and damping coefficient derived by Novak et al (1978) was also plotted in Figure 3 for comparison. It can be concluded that the stiffness and damping coefficient simulated by 'Plaxis 8.2' agree well with the theoretical value.

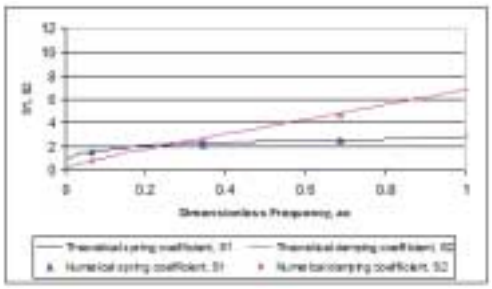

Figure 3.

ELEMENT SIZE EFFECT

The effect of element size is crucial for dynamic calculations, especially for lumped mass finite element codes such as Plaxis. A model with too large element size adversely affects the stress wave propagation. Theoretically, the element size must be as small as possible but it is impractical to adopt very small elements because it increases the calculation time dramatically. Deeks and Randolph (1992) have proposed that for accurate simulation of stress propagation, the node spacing for a line element must be at least 1/12 of TL, the length travelled by the rising portion of the imposed load in the medium.

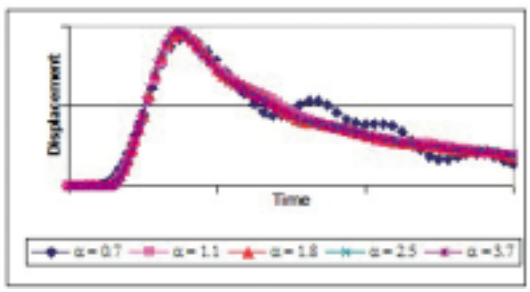

Figure 4.

To assess the optimum element size for a 15-node triangular element, the same mesh in Figure 2 was utilized by replacing the harmonic load with a half sine load with a certain loading duration. Figure 4 plots the displacement trace measured at a distance of 0.5m from the imposed load for the mesh with a different α ratio, defined as

$$\alpha = \frac{T_L}{Average\ Element\ Size}$$

It was found that the measured displacement trace is identical for $\alpha > 1.8$, thus 2 is proposed as the optimum a value.

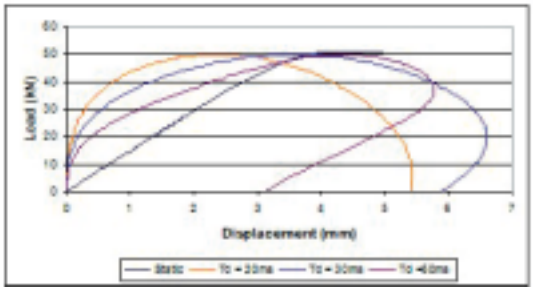

Figure 5.

RESULT AND DISCUSSION

Figure 5 shows the load displacement curves calculated by Plaxis 8.2 for a stiff nail 100mm in diameter and 5m in length loaded by a half sine load with different loading durations. All dynamic loading results fall in the kinetic loading condition with a relative wave length > 10. The numerically simulated static load displacement curve is also plotted in this figure for comparison. This figure clearly shows that the difference between dynamic and static load displacement curves becomes less with longer loading duration.

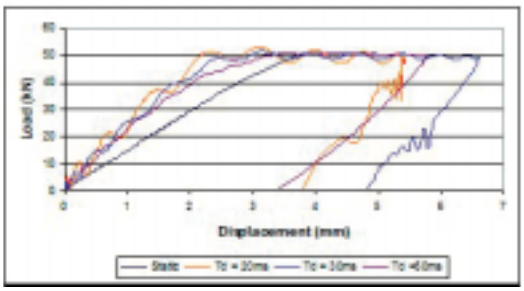

Figure 6.

Figure 6 shows the dynamic soil response curves, which were derived from Figure 5 by subtracting the inertia effects. The inertia effect was assumed equal to the nail's total mass multiplied by the nail's head acceleration, considering that only the nail's head acceleration is measurable in actual field tests. The difference between the soil response curve and the static pullout curve is now purely due to the radiation damping effect. The effect of an increase in the stiffness coefficient due to dynamic loading is negligible as shown in Figure 3.

Figure 7 and Figure 8 show the dynamic soil response and static load displacement curves for a 15m extensible nail, measured respectively at the nail's head and the nail's tip. Again kinetic loading conditions were ensured. These figures show that the dynamic soil response curves are almost similar to the static load displacement curve with insignificant dynamic effects. This is because a longer loading duration (> 60ms) is required to achieve a kinetic loading condition. The dimensionless frequency, a0, for a longer loading duration will be smaller; and the damping coefficient will also be smaller by referring to Figure 3. As an example, for a loading duration of 100ms, the a0 is equal to 0.03 and the damping coefficient is close to zero (Figure 3).

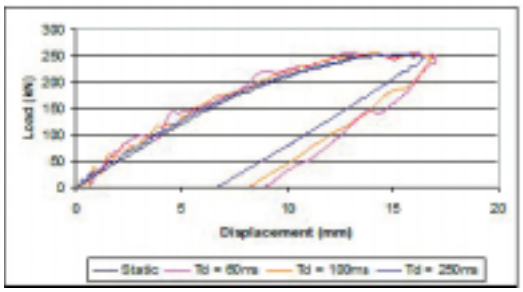

Figure 7.

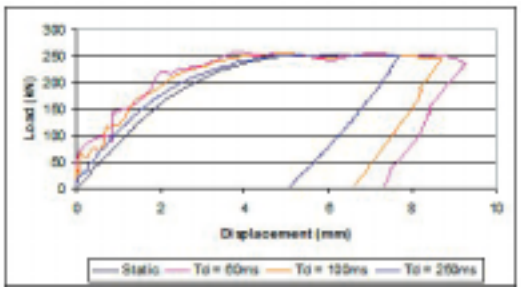

Figure 8.

CONCLUSION

In this article, the dynamic pullout test of a single soil nail was simulated using the Plaxis 8.2 dynamic module. At first, the ability of 'Plaxis 8.2' to accurately simulate the radiation damping effect of a vibrating shaft with an axisymmetric model was examined, and found to be closely comparable with the theoretical solution. From a series of parametric studies on the effect of element size, it is recommended that the α ratio (as defined in this article) should be larger than 2 to ensure the accuracy of stress propagation in this lumped mass finite element program.
The numerically simulated soil nail's dynamic pullout behavior has provided convincing results on the viability of a dynamic pullout test to assess the static pullout behavior of both stiff and extensible nails. Generally the dynamic pullout response is stiffer than the static pullout response, mainly due to the damping effect (radiation damping). The increase in loading duration decreases the damping effect, and consequently the dynamic pullout response will be closer to the static pullout response. For the simulated case, the radiation damping effect is negligible for loading durations > 100ms.

REFERENCES

Chow, Y.K. Dynamic Behavior of Piles. PhD Thesis, University of Manchester. 1981.

Deeks A.J. and M.F. Randolph. Accuracy in Numerical Analysis of Pile Driving Dynamics. In 4th Int. Conf. Application of Stress Wave Theory to Piles, 1992, the Hague, the Netherlands, pp 85-90.

Holeyman, A.E. Keynote lecture: Technolofy of Pile Dynamic Testing. In Proc. 4th Application of Stress Wave Theory to Piles, September 1992, the Hague, the Netherlands, pp 195-215.

Novak, M., T. Nogami and F. Aboul-Ella. Dynamic Soil Reactions for Plane Strain Case. J. Engineering Mechanics Division, ASCE, vol. 104, pp 953-959. 1978.

Randolph, M.F. and P. Wroth. Analysis of Deformation of Vertically Loaded piles. J. Geotechnical Engineering div., vol. 104, pp 1465-1488. 1978

WHAT IS THE MECHANICAL IMPACT OF

Frans Barends, GeoDelft / Delft University of Technology

Water pressures play a crucial role in the stability of dikes and excavations. Stability and deformation incorporating the actual local pore pressures is based on:

equilibrium: $\sigma_{ij,j}' = p_{,i}$ (1)

and can be obtained by PLAXIS. The pore pressure field is conceived as input, as a conditioned volume force. How this field is determined? Figure 1 shows a typical canal embankment near Delft in the Netherlands which conducts the excess water pumped out of the lowlands, here almost 4 meter under the canal water level.

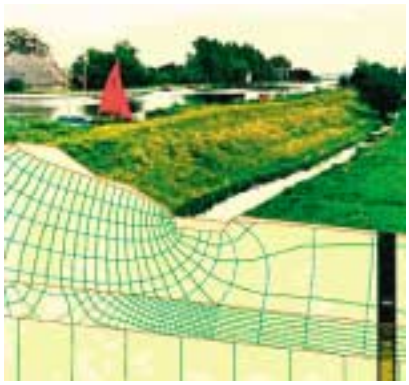

Figure 1: Stagnant flow in a canal embankment.

The stationary groundwater flow pattern in the geological stratification consisting of peat, clay, and sand (top down) can be determined by the porous flow equation:

stat. flow: $K_{ij}(p_{,j} + \gamma z_{,j})_{,i} = 0$ (2)

where anisotropy and inhomogeneity are included in the permeability K.
Capillarity and infiltration by rain, evaporation or overtopping water determine the dynamics of the groundwater table. Then the permeability K is a function of the moisture content θ. This flow field is described by:

unsat. flow: $K[\theta](p_{,i})_{,i} + \gamma K[\theta]_{,z} = \gamma \theta_{,t}$ (3)

For example, infiltration on a sloping surface shows a saturated zone on top and a wetting front propagating vertically, finally reaching the groundwater table underneath (see fig. 2)

Saturated groundwater flow including storage effects, like fluid compressibility β is formulated by:

compr. flow: $K_{ij}(p_{,j} + \gamma z_{,j})_{,i} = n\gamma\beta\, p_{,t}$ (4)

The so-called elastic storage, related to the compressibility of the porous medium: α, can be included in a similar manner:

stor. flow: $K_{ij}(p_{,j} + \gamma z_{,j})_{,i} = S\, p_{,t}$ (5)